Hindawi
International Journal of Antennas and Propagation
Volume 2022, Article ID 4555483, 10 pages
https://doi.org/10.1155/2022/4555483

Research Article

A Method for Predicting Coupling Laws of UWB EMP to Millimeter Wave Detector

Kaibai Chen[1] **and Min Gao**[2]

[1]*Department of Missile Engineering, Army Engineering University (Shijiazhuang Campus), Shijiazhuang 050003, China*
[2]*Department of Missile Engineering, Army Engineering University (Shijiazhuang Campus), Shijiazhuang 050003, China*

Correspondence should be addressed to Min Gao; gaom1101@126.com

Received 15 December 2021; Revised 3 June 2022; Accepted 21 June 2022; Published 6 July 2022

Academic Editor: Angelo Liseno

The millimeter wave detector has been widely applied in short-range detection systems. However, it can be easily disturbed by the ultra-wideband electromagnetic pulse (UWB EMP). In this paper, we proposed a simplified model to investigate the coupling laws of UWB EMP to the millimeter wave detector. With the help of finite integration technology (FIT), the coupling process can be visualized, and the most sensitive pose and the coupling path are analyzed. The irradiation tests are carried out to verify the simulation results. The results show that the shielding effectiveness (SE) of the detector in the vertical state is the worst, and the UWB EMP enters the detector mainly through the circular opening. Under the irradiation of UWB EMP, the detector shows three phenomena: interruptions, constant false alarms, and damage. The interruptions can be recovered by power reset, while the constant false alarms and damage are irreversible effects. The results can be employed to reinforce the electromagnetic compatibility (EMC) of the millimeter wave detector. With the increasing use of short-range detection systems, the EMC of existing products must be improved.

1. Introduction

The millimeter wave detector uses electromagnetic waves to sense targets and has shown great application prospects in short-range detection systems. However, it is sensitive to UWB EMP, which can destroy or jam the detection system through "front-door" and "back-door" coupling effects [1–3]. Nowadays, UWB equipment can be bought by everyone (fast rise time generators or explosively driven systems), and highly sophisticated antennas are available on the public market. With the miniaturization and lightness of UWB generators, terrorist targets could include any civil infrastructure, including private cars, radios, power networks, computer networks, and so on [4]. In consideration of the wide application of short-range detection systems in military and civilian fields, the knowledge of the millimeter wave detector's immunity is of great interest.

Research on UWB effects can generally be divided into two categories: numerical and experimental analysis. Some scholars investigate the coupling effects of complex enclosures and transmission lines with the BLT (Baum–Liu–Tesche) equation [5–9], but the conclusions are difficult to extend to arbitrary enclosures. To solve this problem, researchers established a transfer function between the incident wave and port response by using a random coupling model (RCM). With RCM, one can predict the intracavity coupling effect by obtaining the probability density function of the electric field distribution within the enclosure [10]. The RCM can theoretically be applied to any enclosure, but there are still many issues to be resolved when applied to tiny objects such as millimeter wave detectors.

In terms of experimental studies, there are many detailed investigations into the electronics, involving the following equipment/components: computers and computer networks [11], microprocessor boards [12], the microcontroller [13], logic devices [14, 15], GPS receivers [16], and so on, which are beneficial to studying the UWB effects on the millimeter wave detector. The researchers have obtained susceptibility

levels of those equipment/components through the tests, and some factors that may affect the results are being investigated. Up to the present, a perfect theoretical and experimental system has been constructed through continuous improvement of research methods [17–19].

The effect of UWB EMP on electronic systems is a systematic project. As a complete system composed of many electric components, the susceptibility level of a millimeter wave detector is different from that of a single electric component. Two problems need to be solved in order to verify the susceptibility level. On the one hand, the cost of the UWB facility and UWB test is too expensive. On the other hand, it is hard to measure the internal electric field strength of the equipment under test (EUT), which will cause trouble in the susceptibility analysis. In order to solve these problems, a simplified model of the millimeter detector is constructed, and the most sensitive pose and energy-coupling path are investigated. With this model, the coupling voltage can be extracted and injected into the circuit analysis so that the sensitive part of the detector can be preliminary analyzed. The simulation results are confirmed by the irradiation tests.

This paper is organized as follows: the test facility is briefly introduced in Section 2. In Section 3, the simulation results are presented. In Section 4, the test results are presented. The discussion is shown in Section 5. Finally, the conclusions are given in Section 6.

2. Test Facility

The test facility is shown in Figure 1. It consists of a UWB EMP generator, an electric field monitoring antenna, the EUT, the test bed, and two oscilloscopes placed in the shielding box (SE up to 60 dB). The first oscilloscope, whose bandwidth is up to 20 GHz, is used to monitor the waveform of UWB EMP, and the second is used to record the trigger signal output by EUT.

2.1. The UWB EMP. As described in [4], a pulse has an ultra-wideband spectrum when the bandwidth percent ratio (bw%) is greater than 25%. The bw% is defined as follows:

$$bw\% = \frac{(f_u - f_l)}{f_c} \cdot 100\%, \tag{1}$$

where f_u is the upper-limit frequency, f_l is the lower-limit frequency, and f_c is the center frequency.

The generator can emit the UWB EMP, which is horizontally propagating and vertically polarized. As shown in Figure 2, the electric field strength of the UWB EMP changes exponentially. The rise time of the UWB EMP is about 0.45 ns, which means that the energy can cover a wide frequency range. In addition, the reflection in the field causes the waveform to fluctuate in the tail.

The normalized spectrum of UWB EMP is shown in Figure 3. It can be seen that the UWB spectrum extends from low frequency to 2 GHz. The main spectral peak of UWB EMP is around 360 MHz, and the subspectral peak is around 200 MHz; the energy is mainly concentrated within 1 GHz.

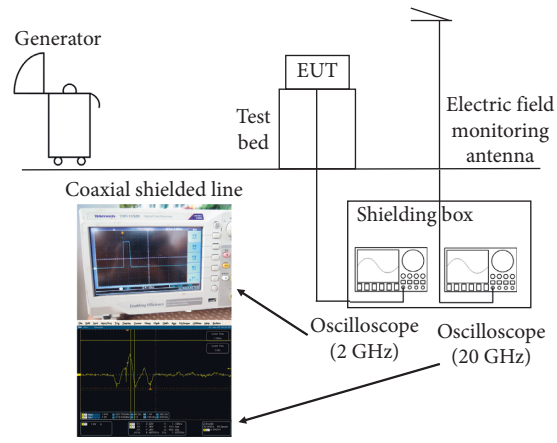

Figure 1: Basic setup of the test facility.

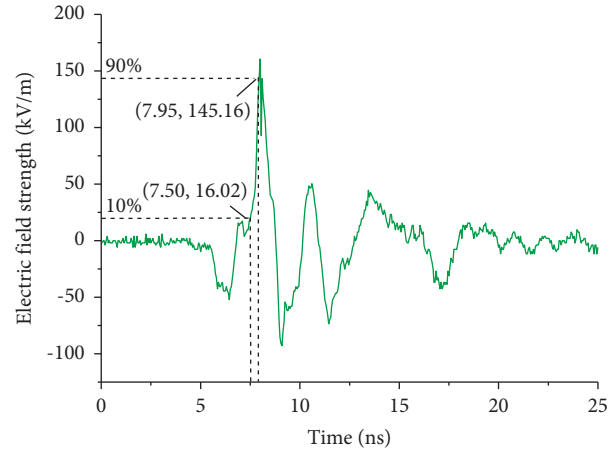

Figure 2: The time-domain waveform of UWB EMP.

Because of the pulley at the bottom of the UWB generator, the distance between EUT and generator can be adjusted flexibly, which is helpful to infer the electric field strength. Figure 4 shows the relationship of measured electric field strength to distance. The relationship can be expressed as follows:

$$E = 718.7e^{(-x/1.54)} + 50.7\,(x \geq 1), \tag{2}$$

where E is the electric field strength and x is the distance between the transmitting antenna and the monitoring antenna.

2.2. The Detector. Figure 5 shows the structure of the millimeter wave detector. The detector is shielded by a metal enclosure. The radio frequency circuit board (RFCB), which is responsible for the signal transmission, is mounted at the top of the enclosure. The metal wires extend outward from the enclosure so that the detector can deal with the power supply and the control signals. The signal processing circuit board (SPCB) for echo analysis is installed inside the enclosure, and the wires are connected to the corresponding nodes. When the detector works, the echo signal is filtered,

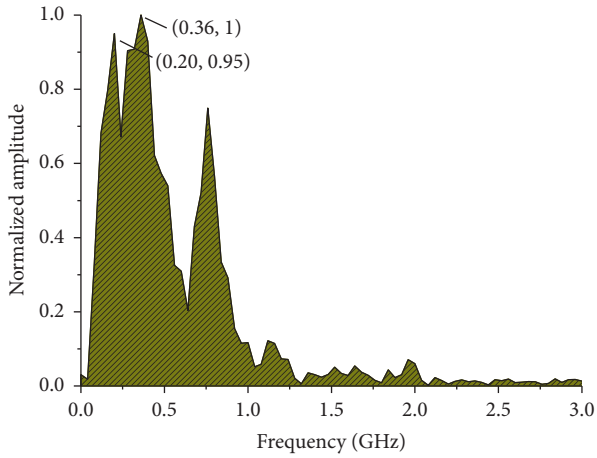

Figure 3: The frequency-domain waveform of UWB EMP.

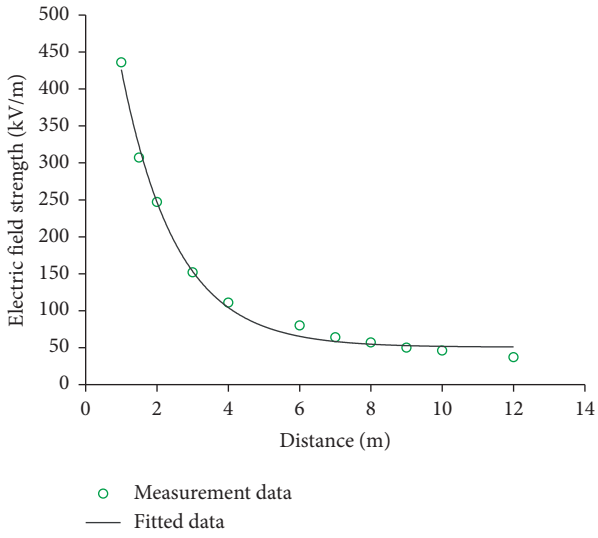

Figure 4: Relation of radiation electric field strength to distance.

amplified, and fed to the SPCB through the metal wire. The signal processing circuit then decides whether or not to output a trigger signal based on the target information.

3. Simulation Analysis

The simulation model is built on CST, which is professional in the field of electromagnetic simulation. CST uses the FIT to calculate the physical fields and has been widely used in the engineering field. The following is a brief description of the FIT.

3.1. Review of Finite Integration Technology. The analytical description of UWB EMP to electronics is very complicated, even if the systems are quite simple. However, numerical approaches can be used to analyze electromagnetic interaction more easily [20]. The FIT was first proposed by Weiland in 1977 [21]. It provides a universal spatial discretization scheme applicable to various electromagnetic problems, ranging from static field calculations to high-frequency applications in the time domain or frequency domain. The FIT is solved numerically by discretizing the Maxwell integral equation as shown in Figure 6. The spatial discretization is completed by two sets of orthogonal grids (primary grid and dual grid).

On the basis of the two grids, Maxwell's equations can be transformed from continuous space to discrete space by allocating electric voltage on the edges of a grid and magnetic voltage on the edges of a dual grid. The allocation of the voltage and flux components on the grid is depicted in Figure 7.

The complete discretized set of Maxwell's grid equations can be expressed in a new form under the finite time-domain integration method as follows:

$$Ce = -\frac{\mathrm{d}}{\mathrm{d}t}b, \tag{3}$$

$$\widetilde{C}h = -\frac{\mathrm{d}}{\mathrm{d}t}d + j, \tag{4}$$

$$Sb = 0, \tag{5}$$

$$\widetilde{S}d = q, \tag{6}$$

where e and h denote the electric voltage and magnetic voltage along primary and dual edges, respectively. The symbols d, b, and j are the electric, magnetic, and current-density fluxes across primary and dual grid faces, respectively. The topological matrices C, $\widetilde{C}$, S, and $\widetilde{S}$ represent the discrete equivalents of the curl operator and the div operator, with the tilde indicating the dual grid. Compared to the continuous form of Maxwell's equations, the similarity between both descriptions is obvious.

3.2. Field Model. In order to obtain accurate calculation results, the simulation model must be as close to reality as possible. But it is almost impossible to model every detail of the structure. As a result, we develop a simplified field model of the detector based on Figure 5. The model is consistent with the original detector in terms of dimension parameters, and the complex wire connections inside the detector are simplified to a single metal wire, which is placed vertically at the edge of the printed circuit board. The RFCB and SPCB are considered as the conductive layers, and the complex via structure is ignored, but the patch antenna and isolator structure in RFCB and the digital chip structure used in SPCB are retained. The field model is shown in Figure 8, and the dimension of it is shown in Figure 9.

In the simulation, the UWB EMP in Figure 2 is used as the irradiation source, and the energy dissipation threshold is −30 dB. The material of the patch antenna and metal pin is pure copper; the metal wire is set as a copper wire; the material of the shielding enclosure is PEC; the thickness of the conductive layer is 1.2 mm; and the material of the enclosure is FR-4. In order to observe the internal field strength of the model, electric field probes are placed in the center of the chip. SE is defined as follows:

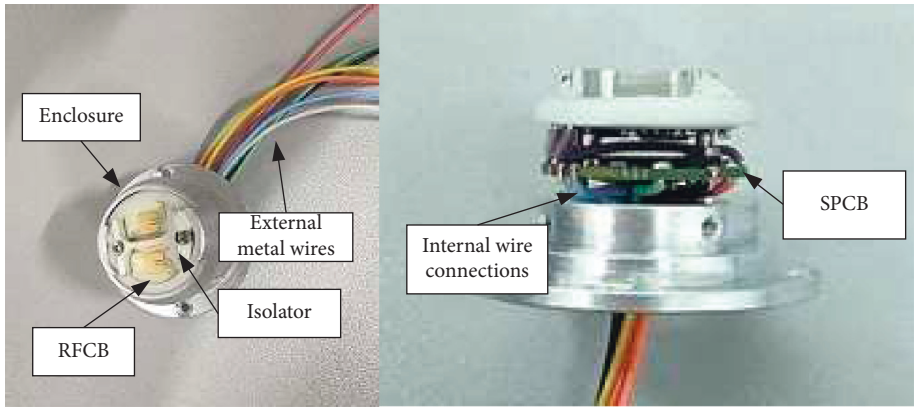

Figure 5: The structure of the millimeter wave detector.

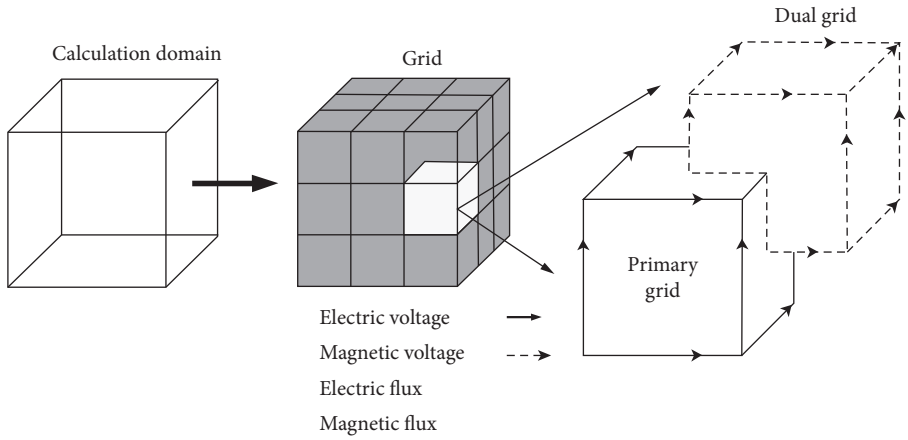

Figure 6: Discrete grid in FIT.

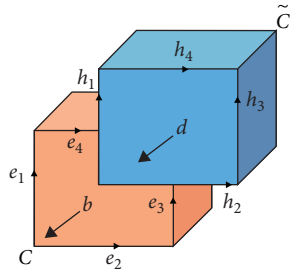

Figure 7: Allocation of the voltage and flux components in the mesh.

$$SE = -20\lg\left(\frac{V}{V_0}\right), \tag{7}$$

where V is the voltage at the observation point inside the detector and V_0 is the voltage at the observation point in the absence of the detector.

3.3. Field Analysis. The coupling effect of the detector at 8.1 ns is calculated, and the electric field distribution is obtained in Figures 10 and 11. As shown in Figure 10, UWB

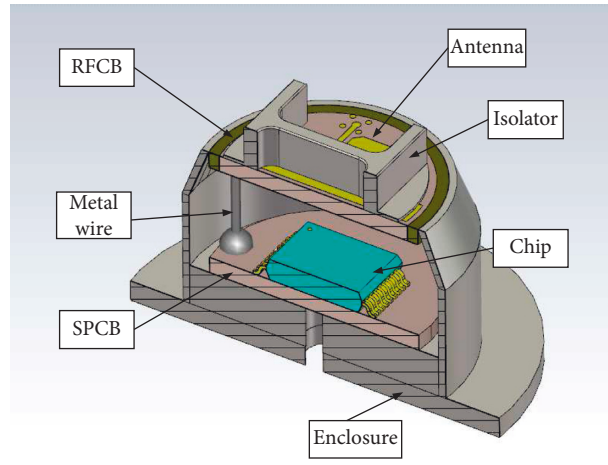

Figure 8: The structure of the field model.

EMP is primarily distributed in the circular opening and gradually attenuates, with an energy density of 1.28 J/m^3. As can be seen from Figure 11, the energy is concentrated at the edges of the upper surface, and the electric field energy density inside the detector is lower than the surface,

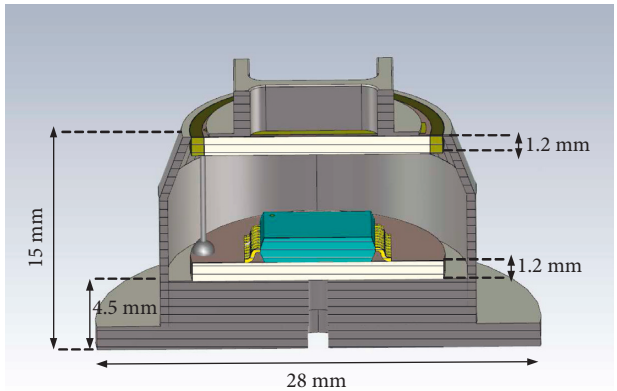

Figure 9: The dimensions of the field model.

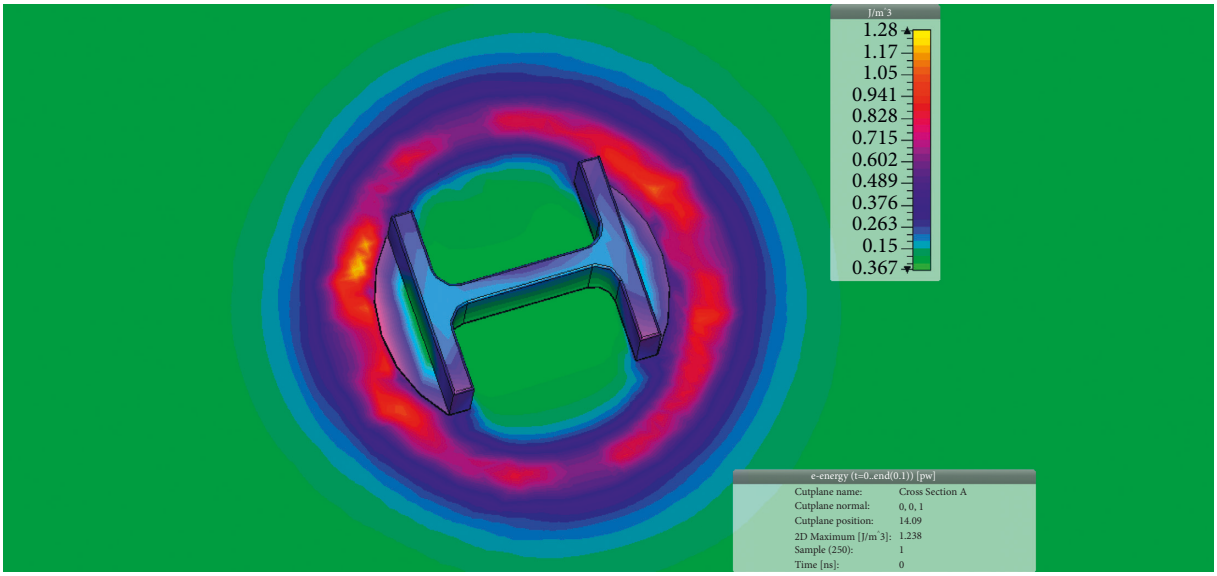

Figure 10: Electric field distribution on the detector surface.

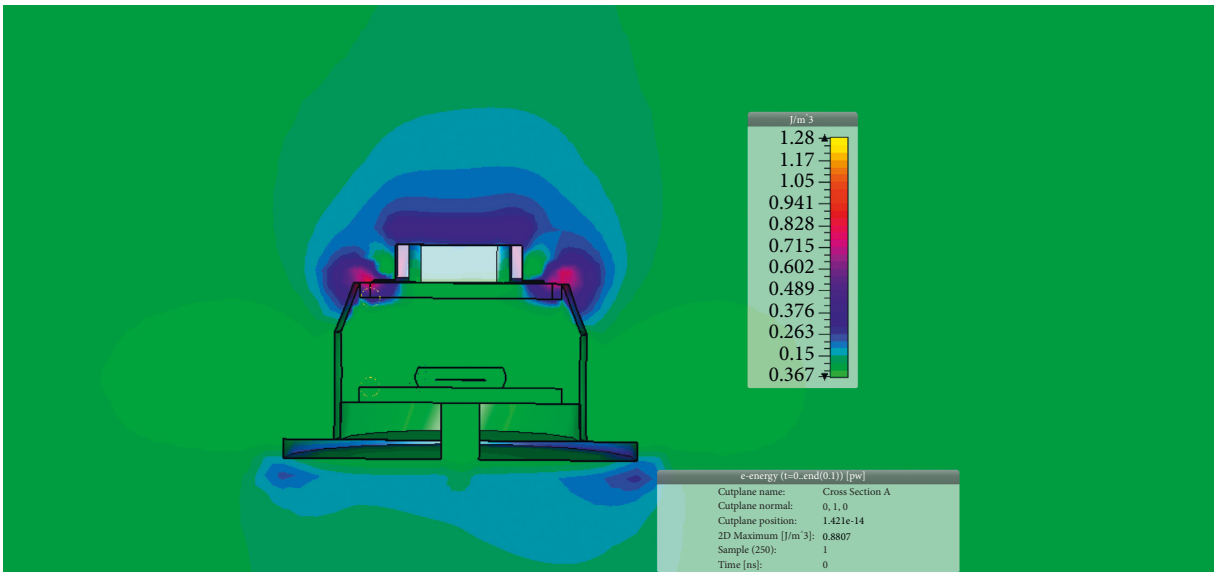

Figure 11: Electric field distribution inside the detector.

indicating that the enclosure has a certain shielding effect on UWB EMP.

As can be seen from Figure 12, the SE of the enclosure gradually decreases as the observation position moves from the center to the circular opening. The maximum difference is 54.63 dB. This indicates that the sensitive elements should be placed at the bottom of the enclosure as far as possible to obtain the best SE in the initial design.

In order to investigate the effects of different incident angles, an electric field probe is placed at the center point of the chip. The X-, Y-, and Z-axis are taken as the rotation axes. As can be seen from Figure 13, the SE remains unchanged when rotating along the Z-axis, and the variation trend of the SE is the same when rotating along the Y- and the Z-axis. The maximum value of SE is 107.98 dB; the minimum value is 20.40 dB; and the difference reaches up to 87.58 dB. The results show that an effective way to avoid the UWB EMP is to change the relative pose between the detector and the UWB EMP.

In addition, it can also be seen from Figure 13 that the most sensitive pose of the detector is the vertical pose. Therefore, the susceptivity in this pose should be paid more attention to when assessing the anti-UWB capability of the detector.

3.4. Circuit Model. The field analysis can clarify the sensitive pose and coupling path of the detector, but it can only provide suggestions on the design in terms of UWB EMP protection, so it is necessary to analyze the sensitive parts of the detector. First of all, we need to know which parts of the detector are sensitive. Based on the electromagnetic field theory, any conductor in the detector can be regarded as an antenna and become a channel for electric field energy conversion and transmission, including patch antennas, metal wires, and metal pins. According to the Friis formula, we can calculate the receiving energy by antenna; if S_r represents the power density at the receiving antenna, it can be obtained by

$$S_r = \frac{P_t G_t}{4\pi R^2}, \tag{8}$$

where R is the transmission distance of the UWB EMP. If the effective area of the receiving antenna is A_{er}, the coupling power of the receiving antenna can be obtained by

$$P_r = \frac{S_r A_{er}}{4\pi R^2}, \tag{9}$$

$$A_{er} = G_r \frac{\lambda^2}{4\pi}, \tag{10}$$

where λ is the working wavelength of the antenna and G_r is the gain of the receiving antenna. Taking the loss factor L_e into consideration, we can obtain the following formula:

$$P_r = \frac{S_r A_{er}}{4\pi R^2} \frac{B_r}{B_t} \frac{1}{L_e} = \frac{P_t G_t G_r \lambda^2 B_r}{(4\pi R)^2 B_t L_e}, \tag{11}$$

where B_r is the bandwidth of the receiving antenna and B_t is the bandwidth of the transmitting antenna.

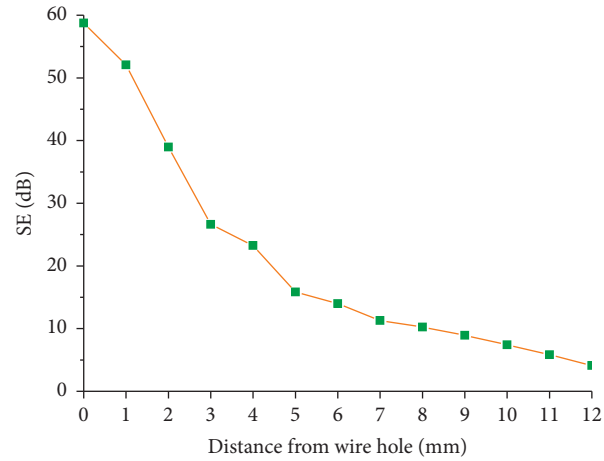

Figure 12: SE of the enclosure.

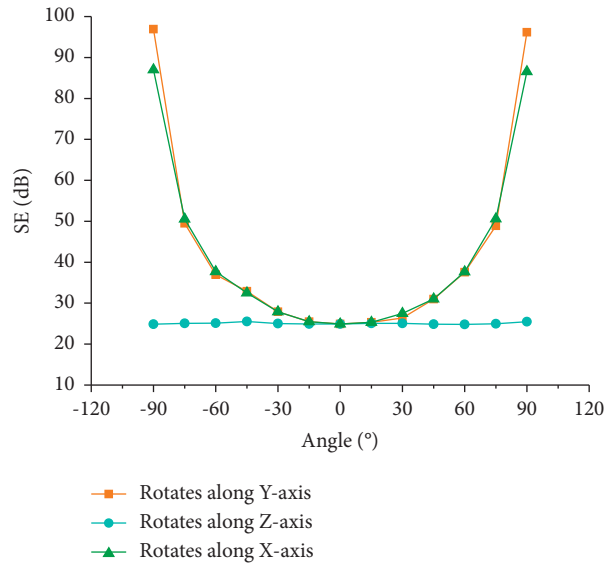

Figure 13: Influence of incidence angle on SE.

It can be seen from (11) that the coupling power is related to many parameters, which are difficult to measure in the tests. However, the coupling power can be easily acquired in the circuit analysis by extracting the induced voltage from the output ports attached to the antenna. As shown in Figure 14, the detector is placed in the most sensitive pose, and the output ports are employed to monitor the coupling voltage of the patch antenna, metal pin, and metal wire.

3.5. Circuit Analysis. As we can see from Figure 15, the coupling power of these parts is different. The peak coupling powers of the metal wire, the patch antenna, and the metal pin are 25.90 dBm, 9.79 dBm, and −2.38 dBm, respectively. The results show that the protection of the metal wire needs to be considered in particular. In addition, we can also see that the coupling effect of the upper end of the metal wire is stronger than that of the lower end. Therefore, the metal wire

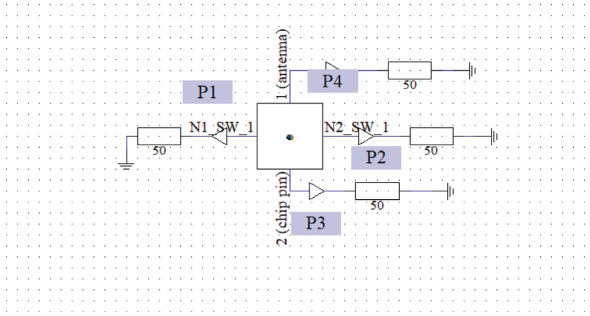

Figure 14: Circuit model.

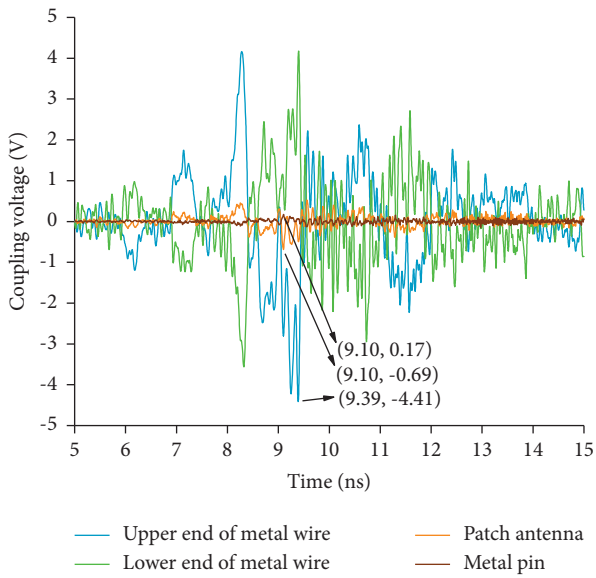

Figure 15: Coupling voltage at sensitive parts.

should be placed at the bottom of the enclosure as far as possible to reduce the induced voltage.

4. Test and Results

4.1. Test Design. In this section, the UWB tests are carried out to verify the simulation results. The general test setup is shown in Figure 16.

In the field test, the detector is placed on the top of a metal cavity, which can provide the power supply for the detector (see Figure 17). The power switch is installed on the side of the cavity. The signal output line of the detector is connected to the coaxial line at the bottom of the metal cavity. The oscilloscope is employed to monitor the trigger signal.

The test steps are as follows:

Step 1. Test the detector to make sure it works.

Step 2. Turn on the power switch and place the EUT in the test field. Start the generator and record the effects data of the detector, then adjust the pose or distance of the EUT, and repeat the tests.

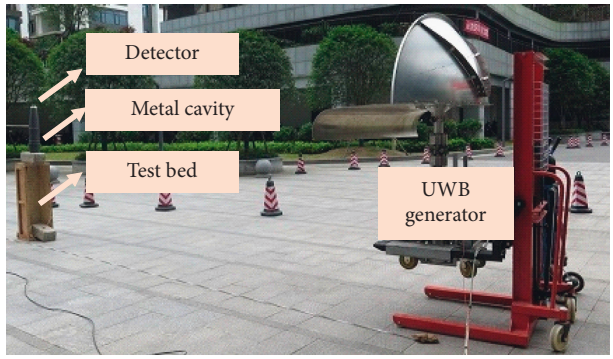

Figure 16: Test setup.

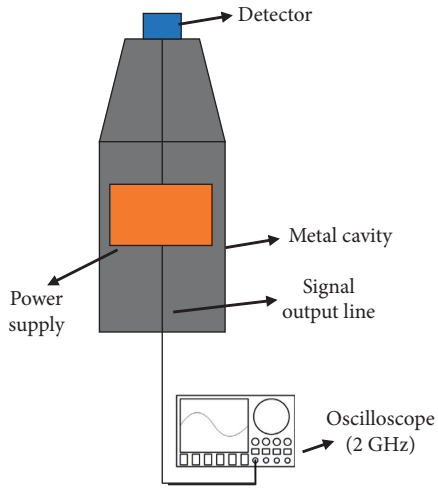

Figure 17: The EUT.

Step 3. Place the EUT in the test field with the most sensitive pose and carry out the test as described in step 2. Record the effect data of the detector and summarize the effects.

The following distinctions were used to differentiate between the different upset events seen during the tests:

(1) Level 0 – No effect observed
(2) Level 1 – Interruptions, recoverable by operation
(3) Level 2 – Constant false alarms, unable to recover
(4) Level 3 – No output signal, unable to recover

4.2. The Most Sensitive Pose. As with the simulation, to verify the most sensitive pose of the EUT, we need to define its pose first. As shown in Figure 18, define (x, y, z) as the rotation angle along the X-, Y-, and Z-axis, respectively, and $(0, 0, 0)$ is the initial pose, indicating that the detector is placed vertically, and the power switch points to the generator.

After defining the pose of the EUT, we use a single pulse to irradiate the EUT. The pulse is triggered five times at an interval of 60 s. Once the interference effect occurs, record the effect level. Figure 19 indicates that the EUT can be disturbed when the electric field strength reaches 150 kV/m. If we want to specify the most sensitive, we need to place the EUT 3 m in front of the UWB generator.

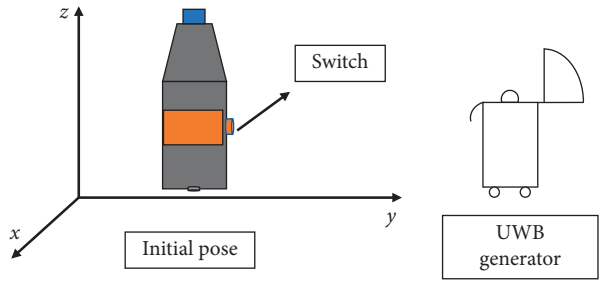

Figure 18: Initial pose of the detector.

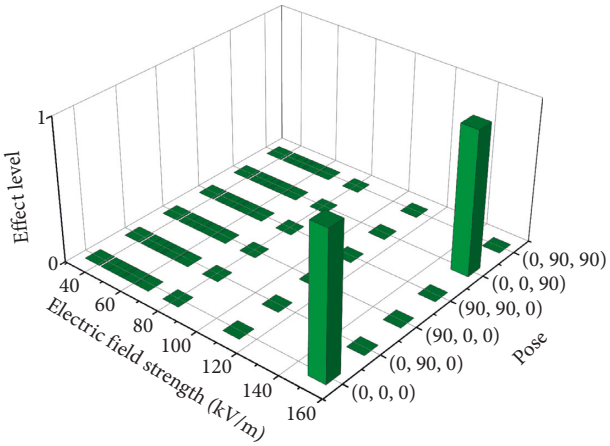

Figure 19: Effect level of the detector.

As we can see from Figure 20, when the EUT rotates along with the Z-axis, the effect level remains. When the EUT rotates along with the X- and Y-axis, the effect level changes in the initial pose. The result indicates that the most sensitive pose of the detector is the initial pose. As described in Section 2, the electromagnetic pulse generated by the UWB generator is a kind of horizontally propagating and vertically polarized electromagnetic wave, which means that the electric field vector of the UWB EMP is perpendicular to the ground plane. Therefore, the UWB EMP can interact with the detector in the amplitude direction when the polarization direction is parallel to the boresight of the detector, making the radiation field strength received by the detector the strongest.

4.3. The UWB Effects. Place the EUT in the field with its initial pose and irradiate it with the UWB EMP. The trigger modes can be divided into the following types:

(1) A single pulse (5 times)
(2) 5 Hz/1 s (5 times)
(3) 25 Hz/1 s (5 times)
(4) 25 Hz/5 s (5 times)
(5) 25 Hz/10 s (5 times)

As can be seen from Figure 21, the UWB EMP cannot affect detector 1 when the irradiation field strength is less than 150 kV/m. When the irradiation field strength increases

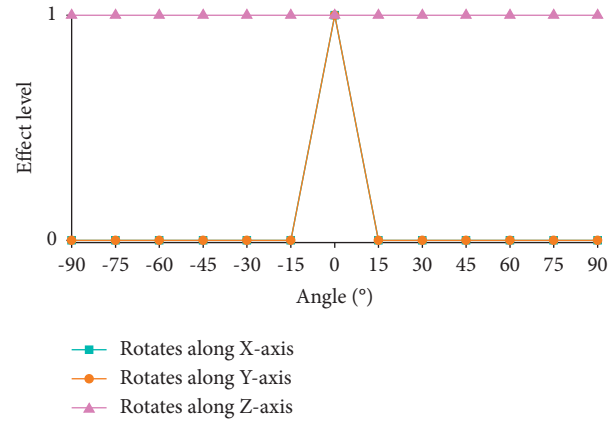

Figure 20: The most sensitive pose of the detector.

to 150 kV/m~360 kV/m, detector 1 is interrupted and can be recovered after a power reset. When the irradiation field strength increases to 436 kV/m, detector 1 outputs the trigger signal after irradiation, and the constant false alarms appear, which cannot be recovered by power reset. The constant false alarms still exist an hour later.

As can be seen from Figure 22, when the irradiation electric field strength is less than 360 kV/m, the effect data of detector 2 is the same as detector 1. When the electric field strength increases to 436 kV/m, detector 2 outputs the trigger signal after the irradiation, and it cannot sense the target after the power reset anymore. Test detector's performance again 1 hour later; the upset event remains; this indicates that the detector may have been physically damaged by the UWB EMP.

Based on the test data above, it can be seen that the threshold of the detector is about 150 kV/m. There is a positive relationship between the effect level and the electric field strength. When the electric field strength increases to 436 kV/m, the detector will appear to have an unrecoverable phenomenon. The effect of the trigger frequency seems unobvious in the test.

A control test is carried out with detector 3 in order to investigate the coupling path of the UWB EMP. We covered the detector with a copper foil shield and did not find any effect on it (see Figure 23). This indicates that UWB EMP enters the enclosure through the circular opening, and the metal cavity is not the coupling path. The conclusion is consistent with the simulation results.

5. Discussion

The results show that the detector is most likely to be disturbed in the vertical state when the UWB EMP is horizontally propagating and vertically polarized. The coupling effect remains unchanged when the detector rotates along the Z-axis. The UWB EMP enters the detector through the circular opening and makes the detector show three phenomena: interruptions, constant false alarms, and damage. The interruptions can be recovered by power reset, while the constant false alarms and the damage are irreversible. The radiation test of sensitive parts is carried out with measured

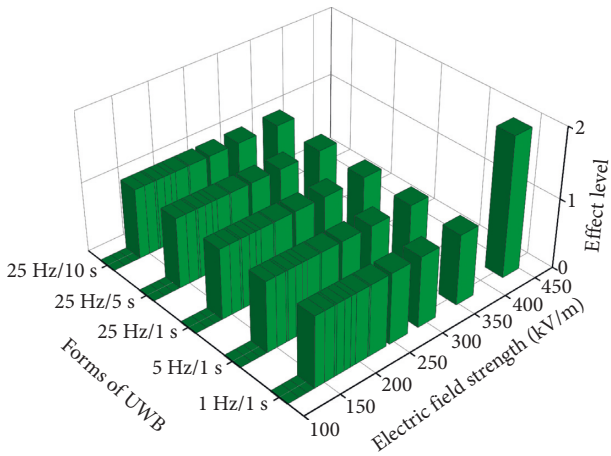

Figure 21: Test data of detector 1.

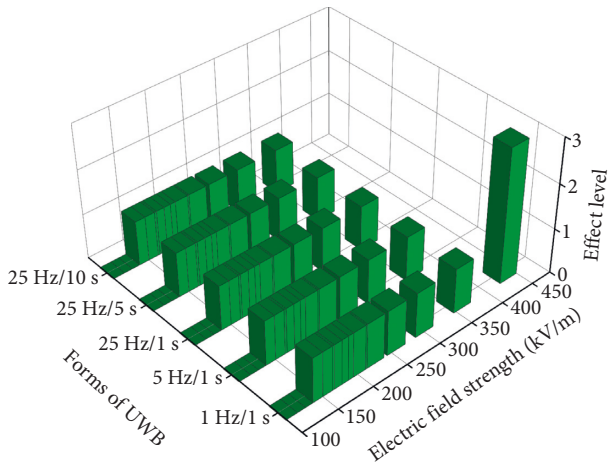

Figure 22: Test data of detector 2.

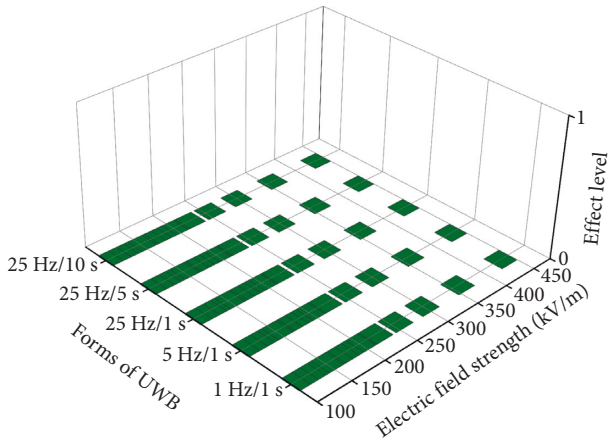

Figure 23: Test data of detector 3 (with shield).

data, and the results show that the metal wire has the highest coupling voltage.

As can be seen from Figure 19, when the detector is placed parallel to the ground and facing the UWB EMP generator, the phenomenon of interruption is disappeared at a distance of 3 m, while when the detector is placed vertically, the effect appears. When the detector is placed vertically, the receiving power of the patch antenna to the UWB EMP is the lowest, so the phenomenon clearly shows that the patch antenna is not the main coupling path of the UWB EMP, and the UWB EMP interferes with the detector in other ways.

Due to the limitation of test conditions, we have not found the specific sensitive parts of the detector. We can only roughly judge that there are electronic components sensitive to UWB EMP on the RFCB or SPCB. In future research, we will conduct a more accurate analysis of the sensitive parts.

The proposed method in this paper is worthy of application and promotion in related research. Combined with the results, the millimeter wave detector should strengthen the ability of anti-UWB interference. Firstly, the dimension of the circular opening could be reduced as much as possible to reduce the coupling energy. Secondly, the components and metal wires should be away from the circular opening. Thirdly, the ability of wire connections to anti-UWB EMP should be strengthened. Simple solutions such as setting a low insertion loss low-pass filter at the sensitive port can be taken into consideration.

6. Conclusion

In this paper, a predicting method is proposed to investigate the effect laws of UWB EMP on the millimeter wave detector. The field analysis and the circuit analysis are carried out to investigate the most sensitive pose of the detector and the coupling path of UWB EMP. Irradiation tests are carried out to verify the simulation results.

Although preliminary research results have been obtained, a large number of tests still need to be continued. In further research, the simulation model needs to be optimized, and other contributing factors to the UWB EMP effects need to be investigated. Besides, we need to strengthen the research on the evaluation method of UWB EMP effects and provide more systematic and comprehensive data for the UWB EMP protection of short-range detection systems.

Data Availability

The data are available from the corresponding author on request.

Conflicts of Interest

The authors declare that they have no conflicts of interest.

References

[1] L. Dongnyok and Y. Keunsig, "A study on the estimation of shelf life for fuze MTSQ KM577A1 from ASRP data," *Journal of Applied Reliability*, vol. 18, pp. 56–65, 2018.

[2] M. G. Backstrom and K. G. Lovstrand, "Susceptibility of electronic systems to high-power microwaves: summary of test experience," *IEEE Transactions on Electromagnetic Compatibility*, vol. 46, pp. 396–403, 2004.

[3] J. D. Zhang, X. J. Ge, Y. W. Zhang et al., "Research progresses on Cherenkov and transit-time high-power microwave sources at NUDT," *Matter and Radiation at Extremes*, vol. 1, no. 3, pp. 163–178, 2016.

[4] F. Sabath, D. Nitsch, M. Jung, and T. Weise, "Design and Setup of an UWB Simulator for Susceptibility investigations," in *Proceedings of the General Assembly of the URSI*, vol. 27, Maastricht, Netherlands, August 2002.

[5] L. Jiang, J. Hao, and Y. Gong, "Analytical method for electromagnetic coupling to a penetrated transmission line in cascaded multiple enclosures with hybrid apertures," *Journal of Electromagnetic Waves and Applications*, vol. 33, no. 7, pp. 1131–1144, 2019.

[6] Y. Gong, J. Hao, and L. Jiang, "Efficient analytical method for the coupling to penetrated transmission line in multiple enclosures based on electromagnetic topology," *IET Science, Measurement & Technology*, vol. 12, no. 3, pp. 335–342, 2018.

[7] H. Tao, C. Dan, F. Farnaz, R. Lingyu, C. Xulai, and W. Jinjin, "Shielding effectiveness analysis and modification of the coupling effect transmission line method on cavities with multi-sided apertures," *Electronics*, vol. 7, no. 4, p. 52, 2018.

[8] A. B. Rabat, D. Bonnet, G. S. Drissi, and S. Girard, "An analytical evaluation of the shielding effectiveness of enclosures containing complex apertures," *IEEE Access*, vol. 9, pp. 147191–147200, 2021.

[9] B. L. Nie, P. A. Du, and P. Xiao, "An improved circuital method for the prediction of shielding effectiveness of an enclosure with apertures excited by a plane wave," *IEEE Transactions on Electromagnetic Compatibility*, vol. 60, no. 5, pp. 1376–1383, 2017.

[10] J. H. Hao, H. D. Pan, and J. Q. Fan, "Application of random coupling model based on time gating method in electromagnetic prediction of complex cavity," *Chinese Journal of Radio Science*, vol. 36, no. 1, pp. 61–67, 2021.

[11] F. Brauer, F. Sabath, and J. Haseborg, "Susceptibility of IT Network Systems to Interferences by HPEM," in *Proceedings of the IEEE International Symposium on Electromagnetic Compatibility*, Austin, TX, USA, August 2009.

[12] C. Mojert, D. Nitsch, H. Friedhoff, and J. Maack, "UWB and EMP Susceptibility of Microprocessors and networks," in *Proceedings of the 14th International Zurich Symposium & Technical Exhibition on Electromagnetic Compatibility*, vol. 14, Zurich, Switzerland, February2001.

[13] M. Camp, H. Garbe, and D. Nitsch, "UWB and EMP Susceptibility of Modern electronics," in *Proceedings of the 2001 IEEE EMC International Symposium. Symposium Record. International Symposium on Electromagnetic Compatibility*, Montreal, Canada, August 2001.

[14] D. Nitsch, M. Camp, F. Sabath, J. L. terHaseborg, and H. Garbe, "Susceptibility of some electronic equipment to HPEM threats," *IEEE Transactions on Electromagnetic Compatibility*, vol. 46, no. 3, pp. 380–389, 2004.

[15] S. M. Hwang, J. I. Hong, and C. S. Huh, "Characterization of the susceptibility of integrated circuits with induction caused by high power microwaves," *Progress In Electromagnetics Research*, vol. 81, pp. 61–72, 2008.

[16] D. MÅnsson, R. Thottappillil, T. Nilsson, O. LundÉn, and M. BÄckstrÖm, "Susceptibility of civilian GPS receivers to electromagnetic radiation," *IEEE Transactions on Electromagnetic Compatibility*, vol. 50, no. 2, pp. 434–437, 2008.

[17] A. Wraight, W. D. Prather, and F. Sabath, "Developments in early-time (E1) high-altitude electromagnetic pulse (HEMP) test methods," *IEEE Transactions on Electromagnetic Compatibility*, vol. 55, no. 3, pp. 492–499, 2013.

[18] R. Rambousky, A. Bausen, S. Lange, and F. Sabath, "IEMI-Testing of Electronic Systems in Critical Infrastructure surrounding," in *Proceedings of the 2015 IEEE International Symposium on Electromagnetic Compatibility*, Dresden, Germany, August 2015.

[19] F. Sabath, S. Koj, and H. Garbe, "Analysis of the coupling of electromagnetic pulses into shielded enclosures of vulnerable systems," *Advances in Radio Science*, vol. 16, pp. 215–226, 2019.

[20] D. Nitsch, F. Sabath, and J. Haseborg, "Susceptibility of Electronic Equipment to Transient Electromagnetic fields of Various waveforms," in *Proceedings of the International Conference on Electromagnetics in Advanced Application*, pp. 213–216, Torino, Italy, September 2001.

[21] T. Weiland, "A discretization method for the solution of Maxwell's equations for six-component fields," *Archiv der Elektrischen Uebertragung*, vol. 31, pp. 116–120, 1977.